Planetary boundary layer and atmospheric turbulence.

Szymon P. Malinowski
Marta Wacławczyk

Institute of Geophysics UW

2017/18

Lecture 08

Flow organization in the ABL, turbulence profiles: Monin-Obukhov scaling and virtual reality of LES simulations.

Turbulence Profiles (Garratt 3.3)

For applications such as the dispersion of pollutants, it is important to understand the characteristics of turbulence in different types of BL. LES simulations illustrate some of these characteristics. Most of the figures below are from Moeng and Sullivan (1994, *JAS*, **51**, 999-1022).

Neutral BLs

Moeng and Sullivan simulated a neutral BL capped by a strong (8 K) inversion at a height of $z_i = 500$ m. The geostrophic wind is 15 m s^{-1} in the $+x$ direction and $u_* = 0.5$ m s^{-1}. The figures on 4.1.4 show x-y slices of u' at various heights, and the wind hodograph. Because of the capping inversion, the wind shear within the bulk of the BL is fairly small (nearly a mixed layer), with strong wind shear across the inversion.

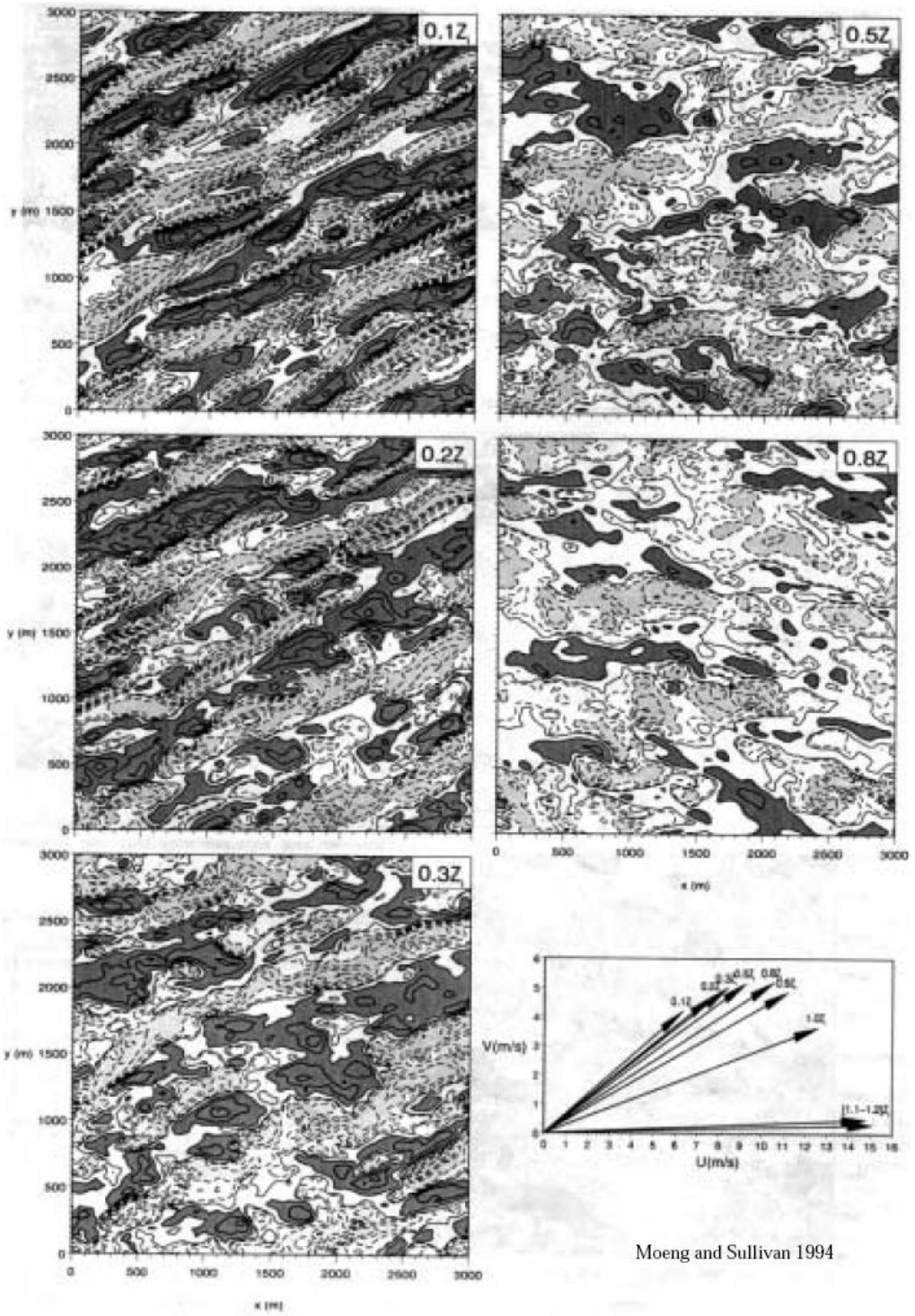

Moeng and Sullivan 1994

FIG. 3. Contours of u in the x–y plane at five height levels for simulation S and its wind hodograph: contours (−3, −2.5, −2, −1.5, −1, −0.5, −0.1, 0.1, 0.5, 1, 1.5, 2, 2.5), dark (light) shading values larger (smaller) than 0.5 (−0.5).

Moeng and Sullivan 1994

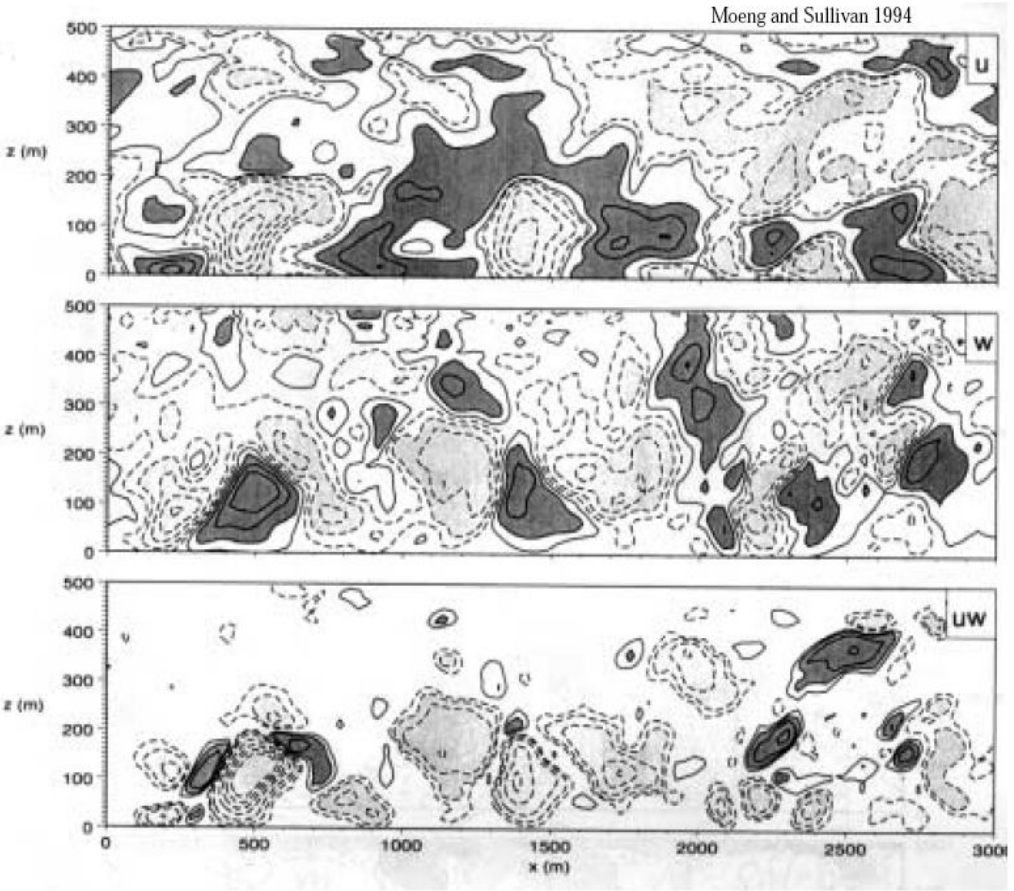

Vertical section through a neutral BL. Note strong anticorrelation between u' and w'.

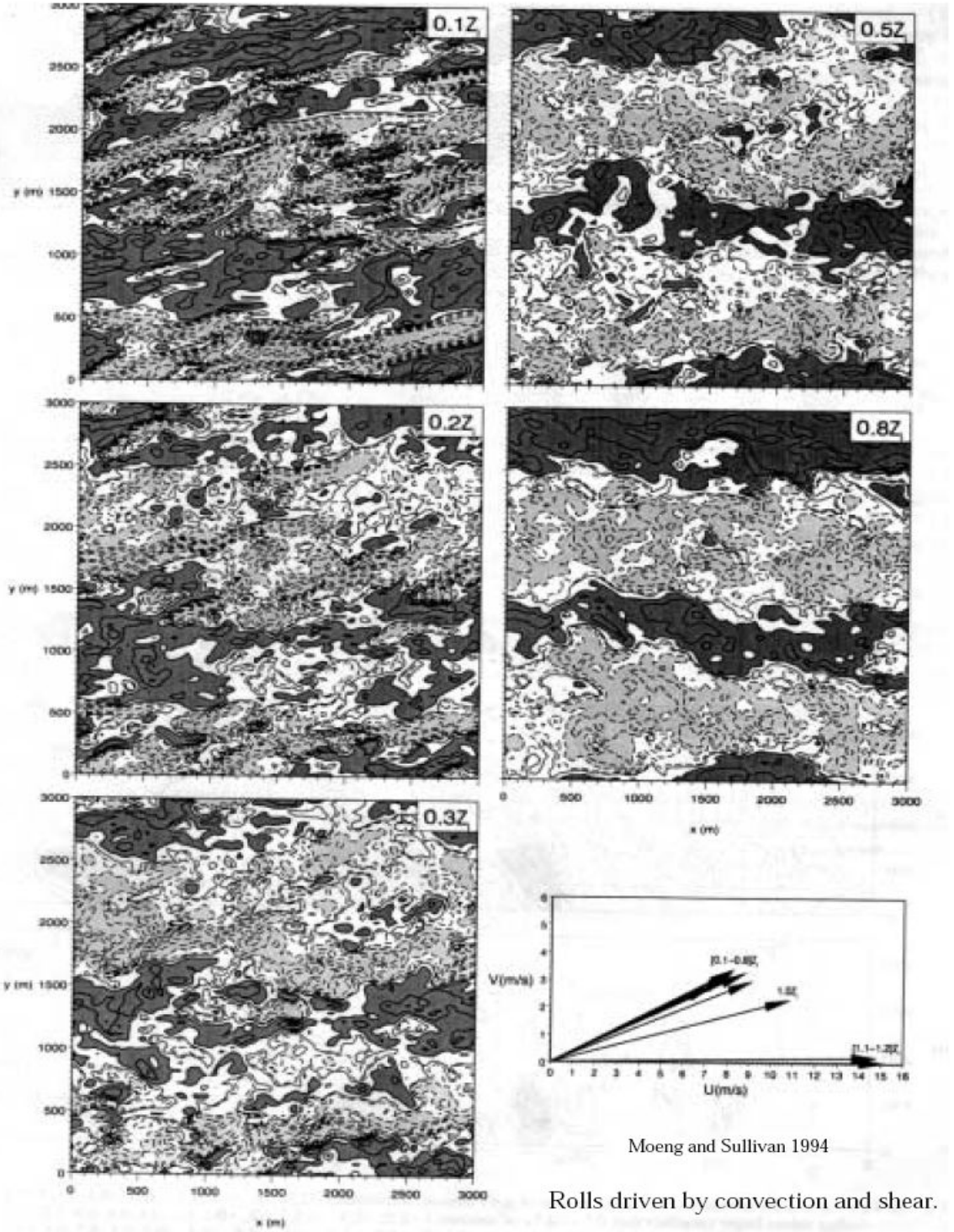

Moeng and Sullivan 1994

Rolls driven by convection and shear.

FIG. 15. Views of x–y for simulation SB1 for u field at five height levels and its wind hodograph: contours (-3, -2.5, -2, -1.5, -1, -0.5, -0.1, 0.1, 0.5, 1, 1.5, 2), dark (light) shading values larger (smaller) than 0.5 (-0.5). Some height labels in the wind hodograph are grouped since winds at those levels are about the same.

Weakly Unstable BLs

Moeng and Sullivan also simulated a weakly unstable boundary layer , also under a capping inversion. This was similar to their neutral case, but with a surface hear flux of 50 W m $^{-2}$, giving an Obuhkov length L = -300 m comparable to z_i. In this case (page 4.1.7), the streaky structure is still apparent at the lowest levels, but large convective rolls dominate the turbulence higher in the BL and help keep it well-mixed. The buoyant and shear contributions to TKE are comparable in this case. A velocity scale based on surface buoyancy flux can be derived from the TKE equation.

$$w_* = (B_0 z_i)^{1/3}$$

(Note that $z_i/L = -kw_*^3/u_*^3$); for this case w_* = 0.9 m s^{-1}. For the buoyancy and shear driven BL a combined velocity scale $w_m^3 = 5u_*^3 + w_*^3$ seems to work best. In particular, with any combination of surface buoyancy flux and shear, Moeng and Sullivan found that the entrainment buoyancy flux is roughly

$$\overline{w'b'}_i = -0.2\ w_m^3/z_i$$

Convective BLs

Lastly, let's look at a purely buoyancy-driven or convective BL. The simulations shown (Moeng and Rotunno 1990, *JAS*) are below a rigid boundary and do not include entrainment, but do show the overall structure well. At the bottom, there is a very good correlation between w' and θ', with polygonal regions of updraft separating circular patches of downdraft. As we move close to the BL top, the updrafts accelerate and combine to become circular, and the temperature fluctuations become much less well correlated with the updrafts. For penetrative convection, in fact the updrafts would be a bit cooler than the surrounding air at the highest level shown.

The velocity variances (previous page) show a very different structure than for a shear-driven BL. They are dominated by the large eddies, which have updrafts in the middle of the BL and predominantly lateral motions at its top and bottom. There is much more velocity variance in the upper part of the BL, so the TKE and TKE dissipation rate are almost uniform with height and equal to $0.4{w_*}^3/z_i$. As in the upper part of a shear-driven BL , about 25% of the TKE generated is going into consumption by entrainment, which averaged over the BL is $\overline{w'b'}_i/2 = 0.1{w_*}^3/z_i$. .

Contrast:

Pure convective BL
- well organized updraft in form of cells.

Is this realistic?

… more in few weeks.

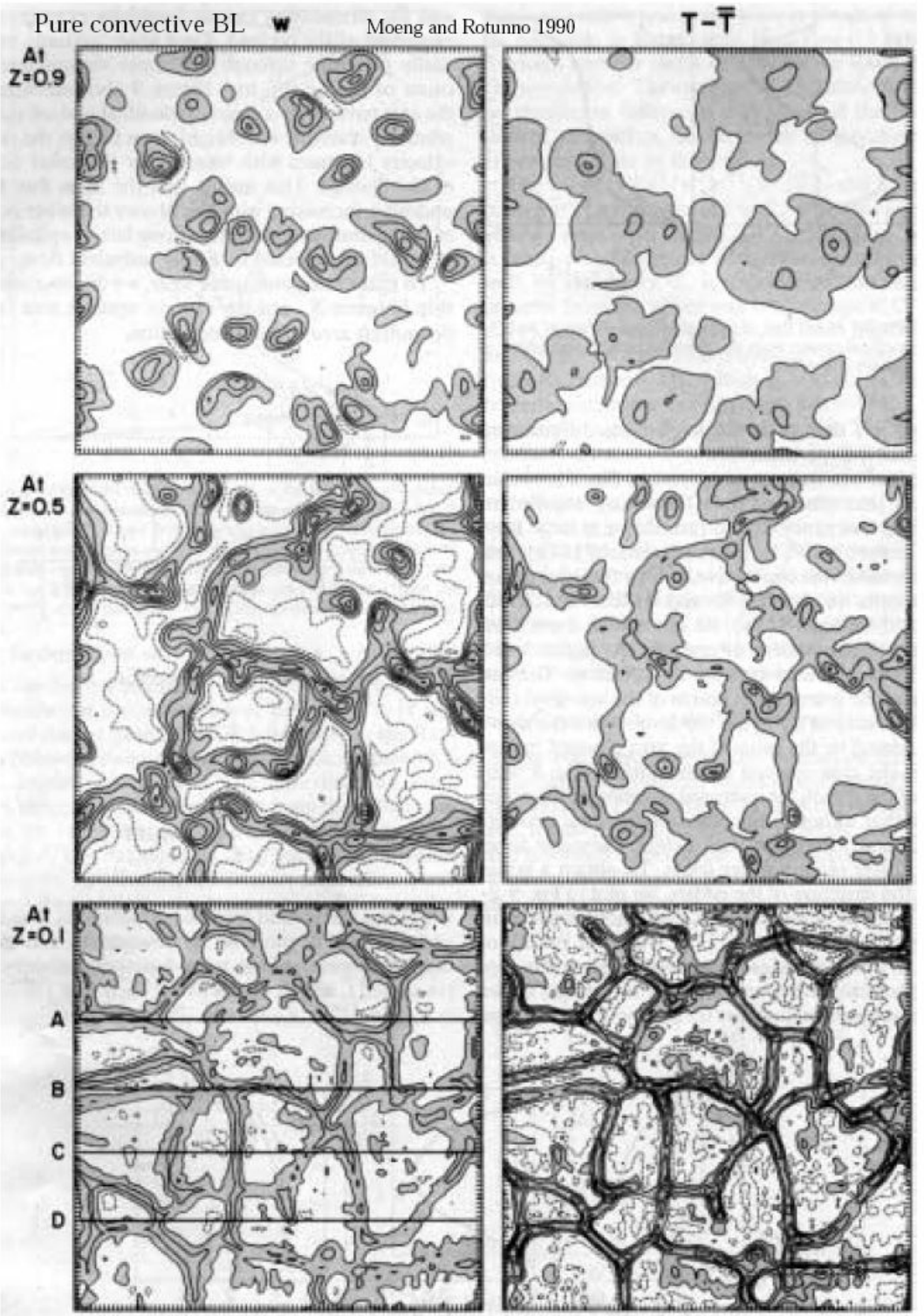

FIG. 8. As in Fig. 3, except for Experiment H. Vertical cross sections through the locations marked A, B, C and D are shown in Fig. 9.

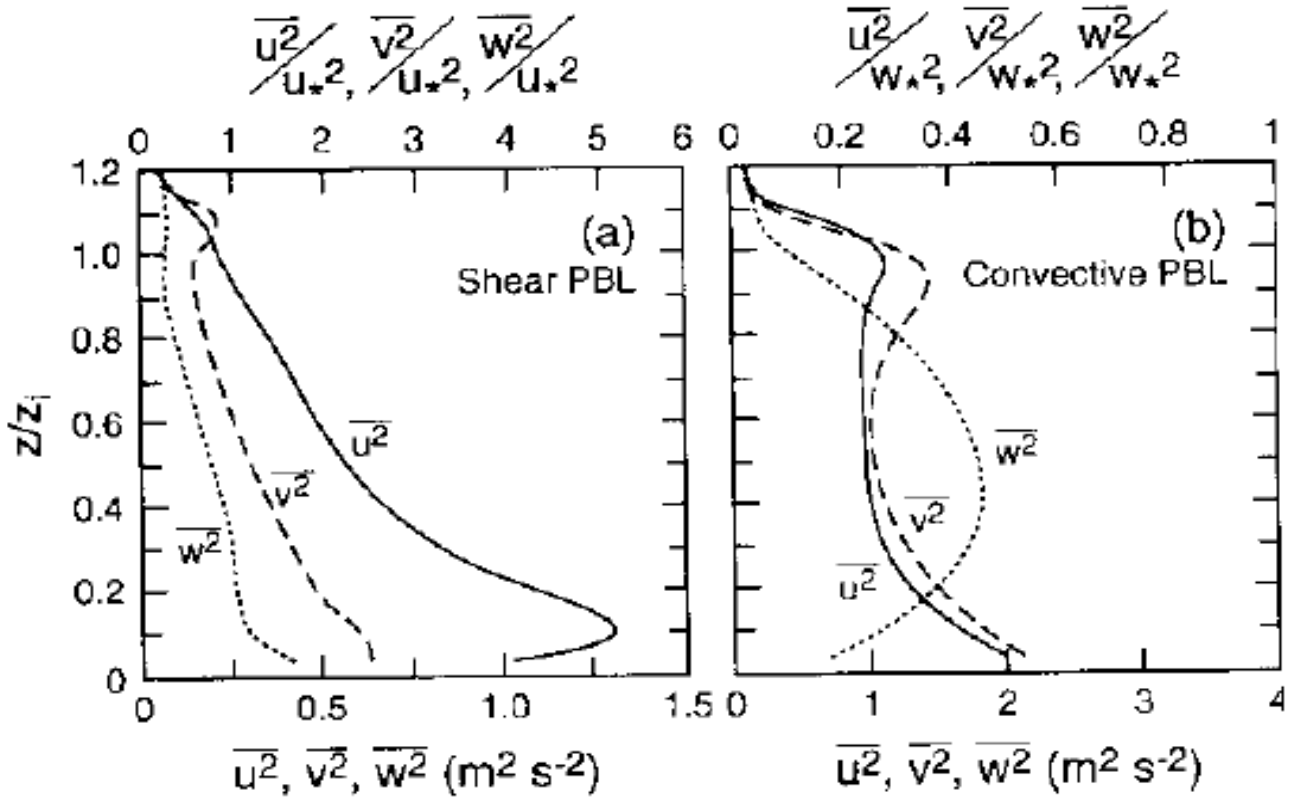

FIG. 9. Vertical distributions of the velocity variances of simulations S and B.

The variances of the three velocity components are shown on the next page, along with their counterparts for a convective BL. For a neutral BL, they are all strongest near the ground, with the strongest perturbations in u at all levels. Their sum, divided by two, is the TKE profile. As we have discussed already, the TKE budget is essentially a balance between shear production (most of which occurs in the lowest 20% of the BL where shear and momentum fluxes are both largest) and turbulent dissipation, with little contribution from turbulent transport.

Although there is no surface buoyancy flux, the turbulence does erode the capping inversion, creating a small downward entrainment buoyancy flux $\overline{w'b'}_i$. In fact, we find that

$$\overline{w'b'}_i = -u_*^3/z_i$$

If we assume that the whole boundary layer is warmed equally by entrainment of warm air from above the inversion, we can associate a buoyancy flux profile with the entrainment which varies linearly from 0 at $z = 0$ to $\overline{w'b'}_i$ at the inversion. The consumption rate of TKE by this buoyancy flux, vertically averaged over the BL, is $\overline{w'b'}_i/2 = -0.5u_*^3/z_i$. If we compare this to the overall dissipation rate of TKE, we find that the TKE dissipation rate is much larger than this at the surface but about $2u_*^3/z_i$ in the upper part of the BL; i. e. entrainment is consuming around 25% of the TKE generated in this region.

Diurnal cycle of the ABL

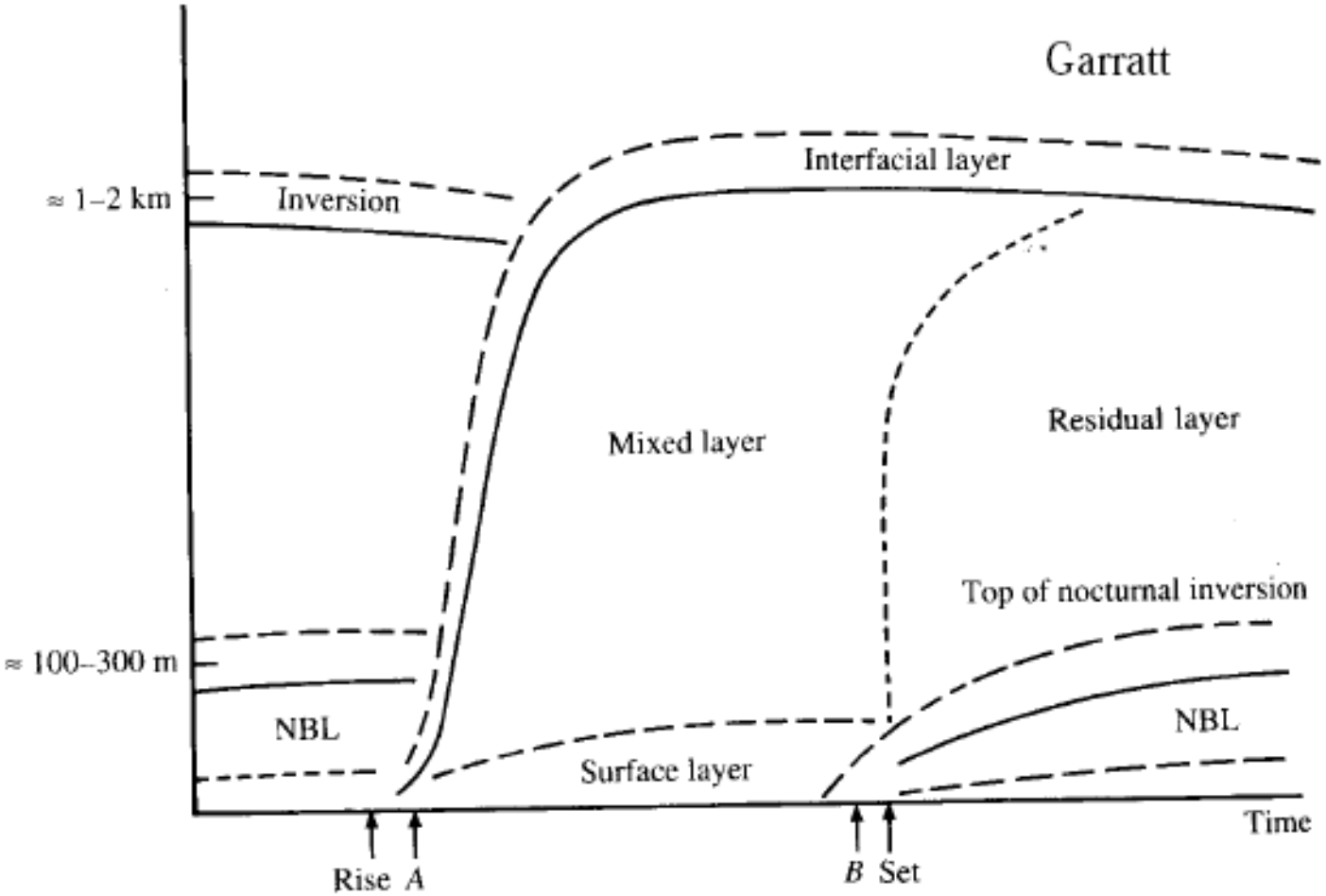

Fig. 6.1 Schematic representation of ABL evolution throughout the diurnal period over land under clear skies.

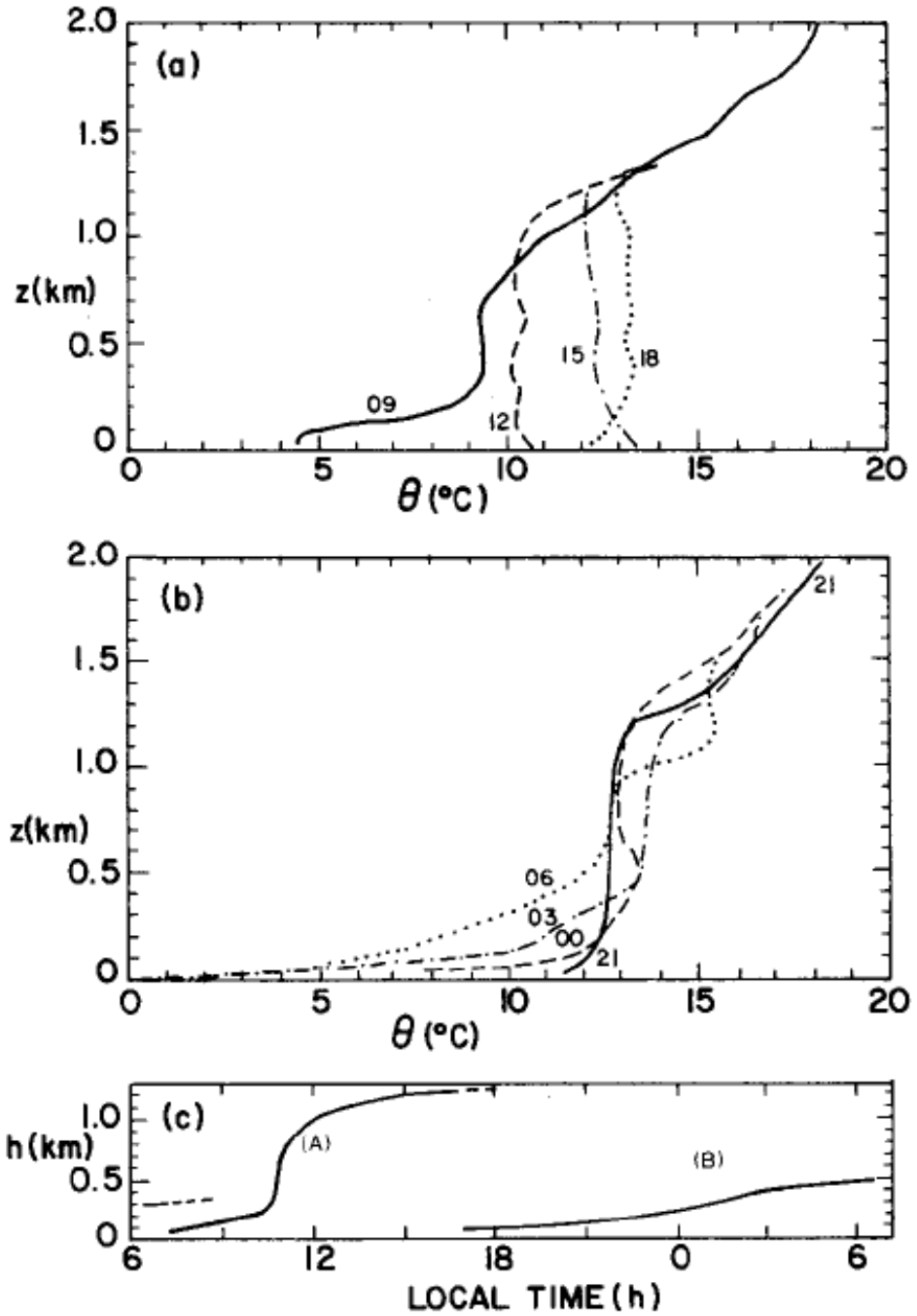

Fig. 5.2 Diurnal variation of potential temperature profiles and the PBL height during (a) day 33 and (b) days 33–34 of the Wangara Experiment. (c) Curve A, convective; Curve B, stable. [After Deardorff (1978).]

Piotrowski, Z., 2008 thesis

e. The ambient potential temperature profile is specified in terms of stratification S as $\theta_a(z) \equiv \theta_b(z) = \theta_o \exp(Sz)$, with assumed surface value $\theta_o = 293.15$ K and buoyancy frequency $N = (gS)^{1/2} = 0.012$ s^{-1}. The uniform ambient wind $\mathbf{v}_a = [-10, -10, 0]$ ms^{-1} is directed from the north-east. Convection is driven by constant surface heat flux $H_o = 0.2$ Kms^{-1}

The model domain is resolved with $nx \times ny \times nz = 127 \times 127 \times 180$ uniform grid intervals $\Delta x = \Delta y \approx 500$ m and $\Delta z = 50$ m, respectively. The simulation is carried out for $t = 6$ h of physical time,

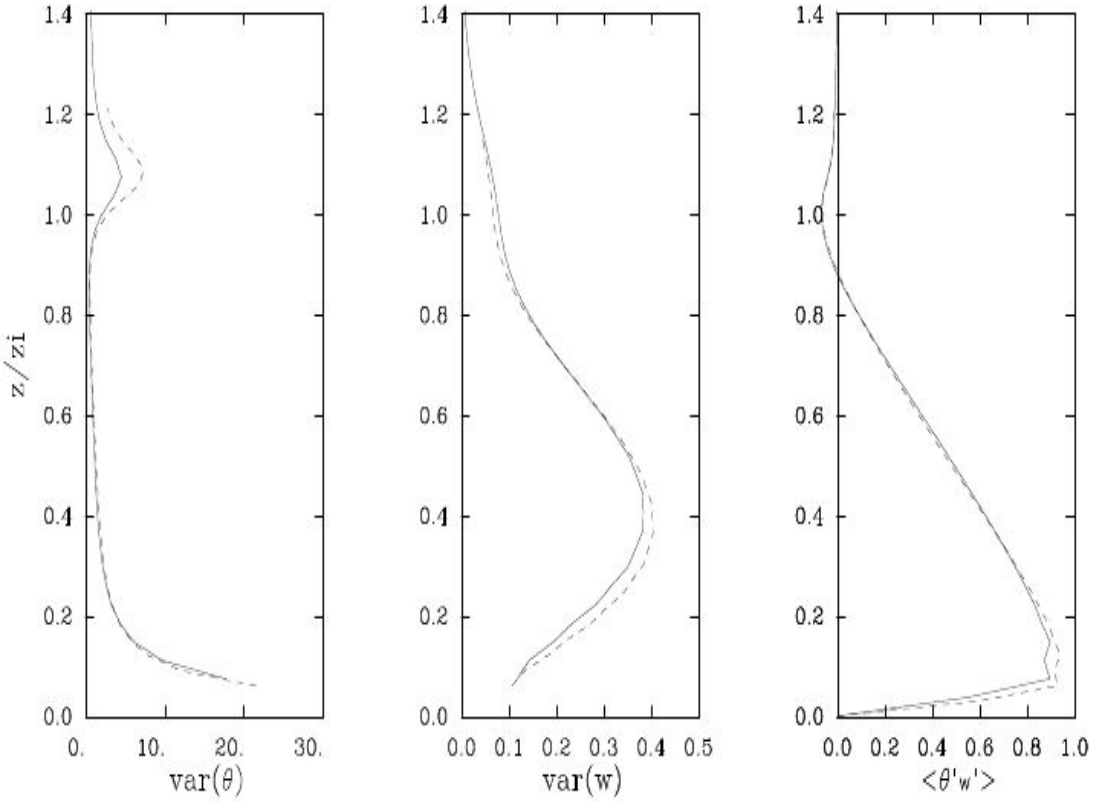

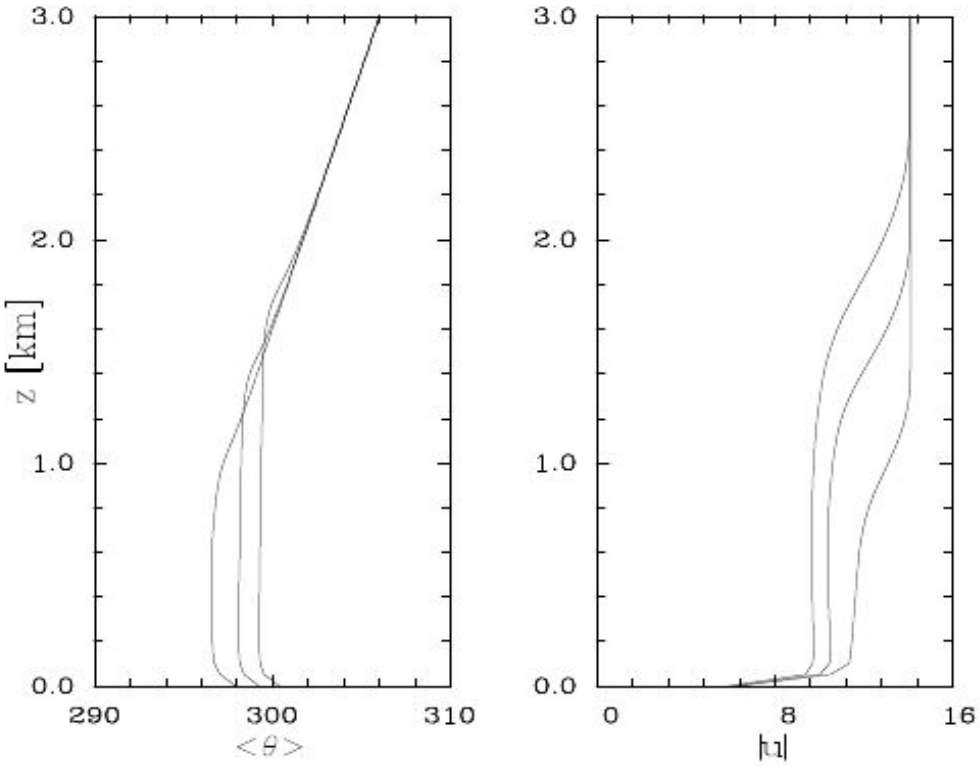

FIGURE 4.2.1. Reference simulation: profiles of horizontally averaged field of potential temperature θ and horizontal wind speed $\sqrt{u^2 + v^2}$ at $t = 2$, 4, and 6 h.

FIGURE 4.2.2. Dimensionless profiles of temperature and vertical velocity variance (left and center) and of turbulent heat flux (right), at $t = 4$ (solid) and 6 h (dashed).

Below are shown LES simulations (Sullivan et al. 1998, *JAS*) of the top of a convective BL penetrating a moderate inversion of 4 K (grid resolution at top right of each plot). White indicates $\theta < 304$ K, other shades increasing θ up to 308 K. Arrows indicate velocity in the x-z plane. Plots show a sequence of times 10 s apart. Note the undulations in the BL top, with downward moving air on the edge of hummocks where updraft air has partly mixed with free-tropospheric air. These motions produce the negative buoyancy flux in the entrainment zone, which for a pure convective BL reaches $-0.2B_0$. Also note in panels e-h the formation of an 'entrainment tongue' at $x = 1750$ m of partly mixed, buoyant air that is getting sucked into the BL.

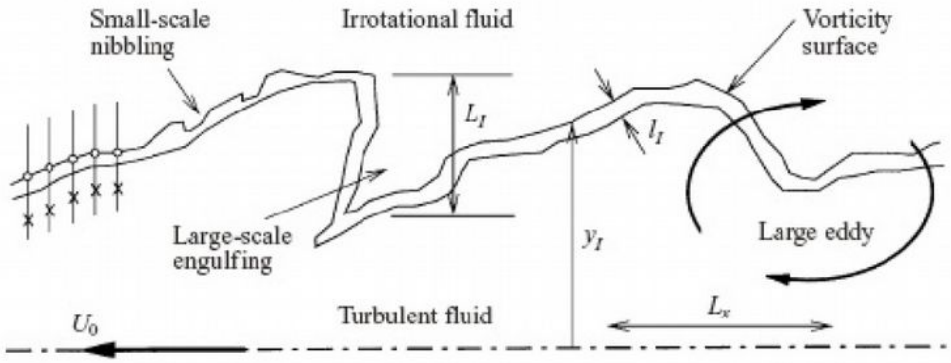

Bisset DK, Hunt JCR and Rogers MM, 2002.

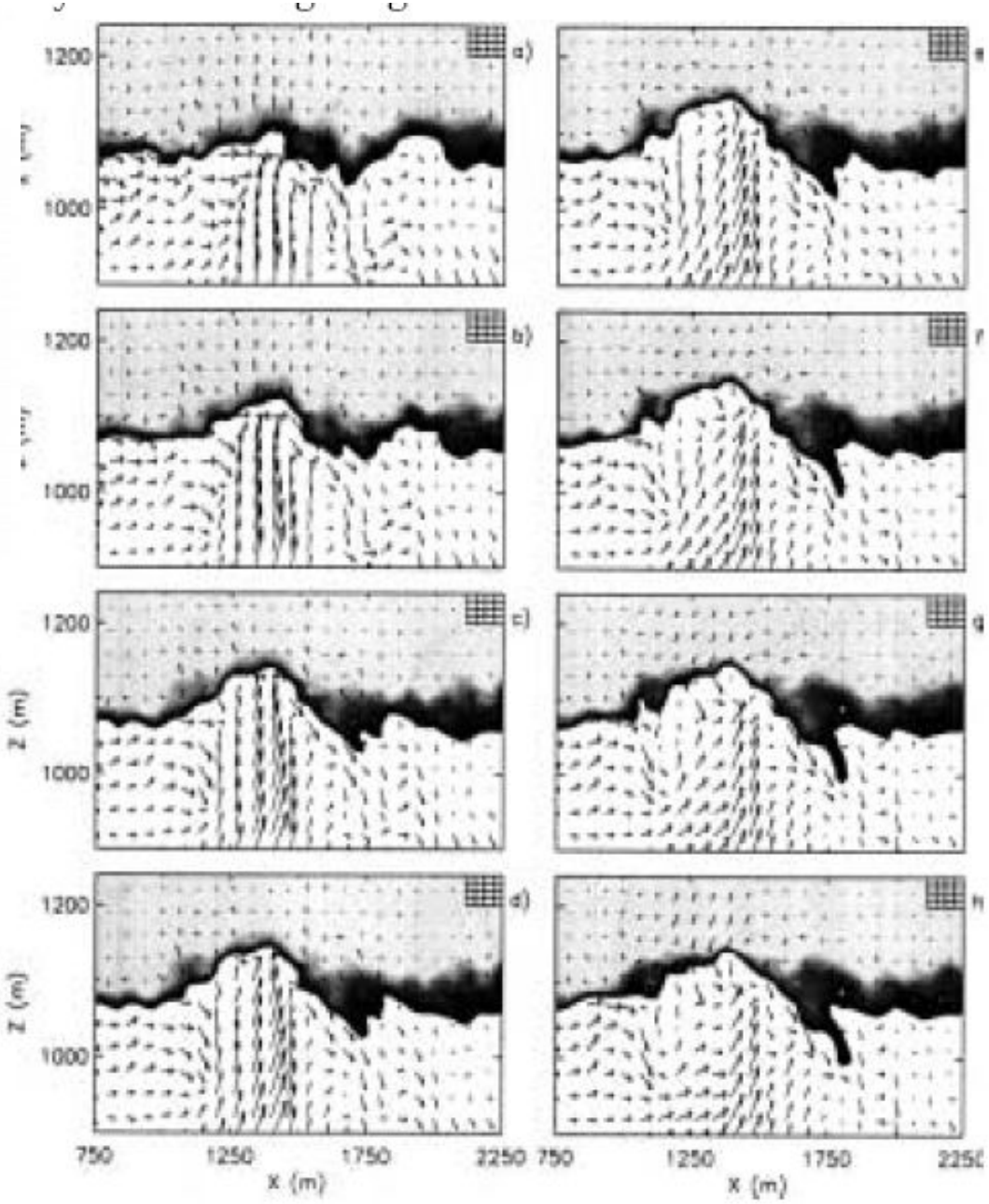

Morning growth of the boundary layer (Garratt 6.1)

The rate of growth of the convective mixed layer is dictated primarily by energy balance, though entrainment dynamics also play a significant role. As a simple example, consider the growth of a mixed layer driven by a surface buoyancy flux B_0 into an atmosphere of constant buoyancy frequency N^2. The mean buoyancy profile in the free troposphere is

$b^+(z) = N^2 z$ (= $g(\theta_v^+(z) - \theta_{vR})/\theta_{vR}$, where we have chosen θ_{vR} as the initial θ_v^+ at $z = 0$.)

We assume (i) that the buoyancy flux is turned on at time $t = 0$, and (ii) that it leads to a convective mixed layer of depth $h(t)$ governed by the entrainment closure

$$\overline{w'b'}(h) = -w_e \Delta b = -\beta B_0 \quad (\beta = 0.2, \text{ empirically}) \tag{1}$$

It is interesting to compare the solution with a realistic β to the case $\beta = 0$. In the latter limit, called **encroachment**, convection is assumed not to be penetrative, and the mixed layer entrains air only when its buoyancy is no larger than that of the mixed layer air. Lastly, (iii) we neglect any mean vertical motion within the atmosphere, so

$$w_e = dh/dt$$

The buoyancy $b(z, t)$ obeys

$$\partial b/\partial t = -\partial/\partial z(\overline{w'b'})$$

Integrating from the surface up to a fixed height H above the mixed layer top, we see that

$$\frac{\partial}{\partial t}\int_0^H b\,dz = -\overline{w'b'}\Big|_0^H = B_0$$

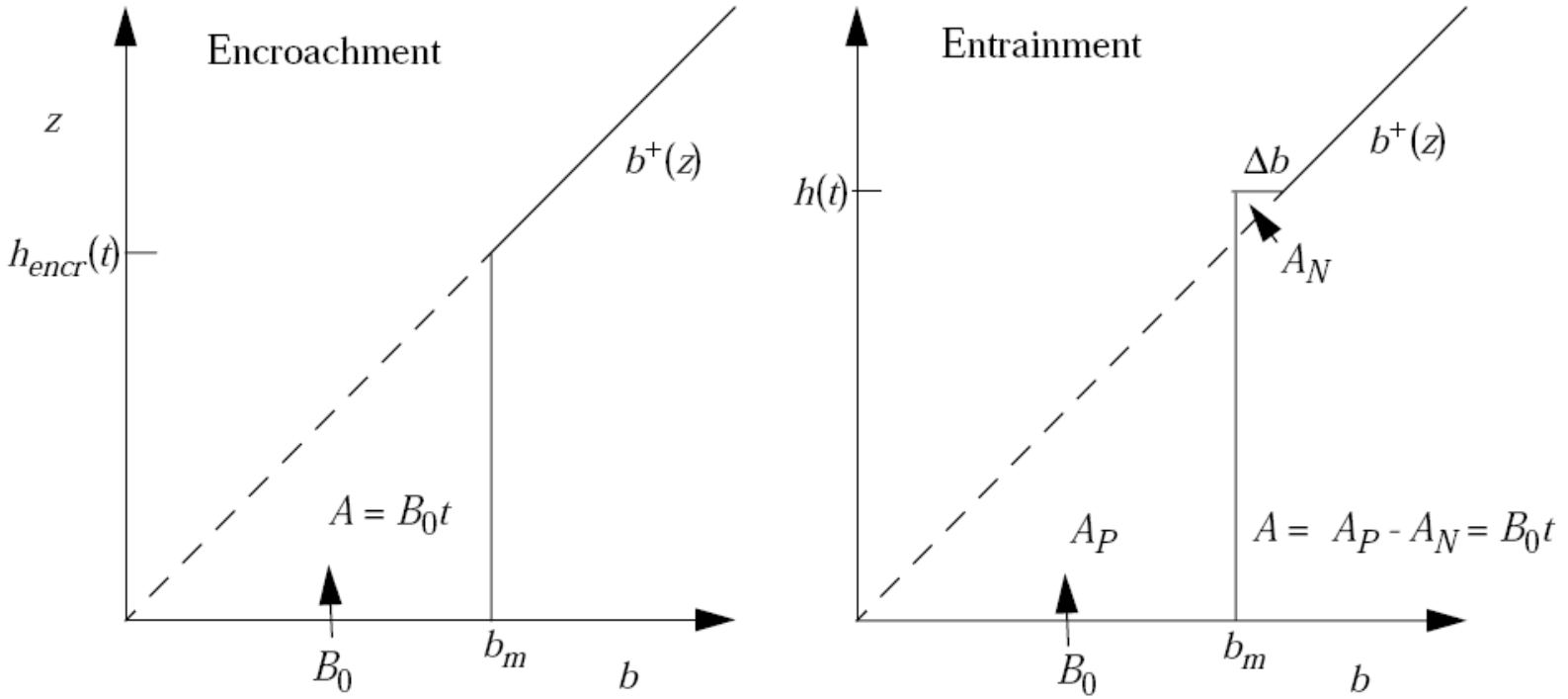

Convective mixed layer evolution illustrating more rapid deepening if entrainment is assumed to be penetrative ($\beta = 0.2$), compared to encroachment ($\beta = 0$).

Graphically, let A be the net area added to the buoyancy profile by the heating of the BL. Then

$$A = B_0 t \tag{2}$$

We can now compare the cases of encroachment and an entraining boundary layer. The encroaching BL has depth given by

$$h(N^2 h)/2 = A = B_0 t \quad \Rightarrow \quad h_{encr} = (2B_0 t/N^2)^{1/2}$$

As expected, h deepens more slowly as it gets larger, since more heat must be imparted to a deeper boundary layer to raise its buoyancy by a given amount.

We can now compare the cases of encroachment and an entraining boundary layer. The encroaching BL has depth given by

$$h(N^2h)/2 = A = B_0t \quad \Rightarrow \quad h_{encr} = (2B_0t/N^2)^{1/2}$$

As expected, h deepens more slowly as it gets larger, since more heat must be imparted to a deeper boundary layer to raise its buoyancy by a given amount.

For the entraining BL, there is a 'similarity' solution in which the buoyancy profile retains the same shape as it grows, so that

$$\Delta b(t) = cN^2h(t) \quad (c \text{ is an as yet unknown constant}).$$

Consistency of (1) and (2) determines c. From (1),

$$\beta B_0 = w_e\Delta b = (dh/dt)cN^2h.$$

Integrating this equation from time 0 to t, starting with $h(0) = 0$, we get

$$\beta B_0t = cN^2h^2/2 \qquad (3)$$

Turning now to (2), we write A as the difference of the 'positive area' A_P where the mixed layer buoyancy $b_m(t)$ exceeds the original environmental buoyancy and the negative area A_N where penetrative convection has reduced the buoyancy. From the figure above, we see that $b_m + \Delta b = b^+(t) = N^2h$, so $b_m = (1\text{-}c)N^2h$. The heights of the triangles making up A_P and A_N are N^{-2} times as long as their bases, so the area of A_P is $b_m(b_m/N^2)/2$ and similarly for A_N. Hence (2) can be written:

$$B_0t = A = A_P - A_N = b_m^2/2N^2 - \Delta b^2/2N^2 = [(1\text{-}c)^2 - c^2]N^2h^2/2 = (1 - 2c)N^2h^2/2. \qquad (4)$$

Dividing (3) by (4), we see that $\beta = c/(1 - 2c)$, or that $c = \beta/(1 + 2\beta)$. It follows from (4) that

$$h_{entr} = (2B_0t/N^2(1 - 2c))^{1/2} = (2B_0t(1 + 2\beta)/N^2)^{1/2} \approx (1 + \beta)\,h_{encr}$$

We conclude that entrainment contributes about $\beta = 20\%$ to the boundary layer deepening. For a 1 km deep BL and $N^2 = 10^{-4}$ s^{-1}, the inversion strength would be $\Delta b = .14N^2h \leftrightarrow \Delta\theta_v \approx 0.4$ K, regardless of the surface buoyancy flux. Entrainment hardly changes the boundary layer temperature.

The nocturnal jet

As turbulence dies down in the residual layer in late afternoon, it decouples from the BL. The momentum flux convergence that was helping to reduce and turn the wind during the day suddenly disappears, leaving a wind profile in which there is an imbalance between the two main horizontal forces, Coriolis force and pressure gradient force. The figure below shows the resulting evolution of the wind during one night of the Wangara experiment (which took place over flat ground). During the night a strong jet develops above the nocturnal BL. In the bottom panel is another example in which the geostrophic wind is also plotted. During the daytime, the wind component along the geostrophic wind direction is subgeostrophic, but at night it is supergeostrophic.

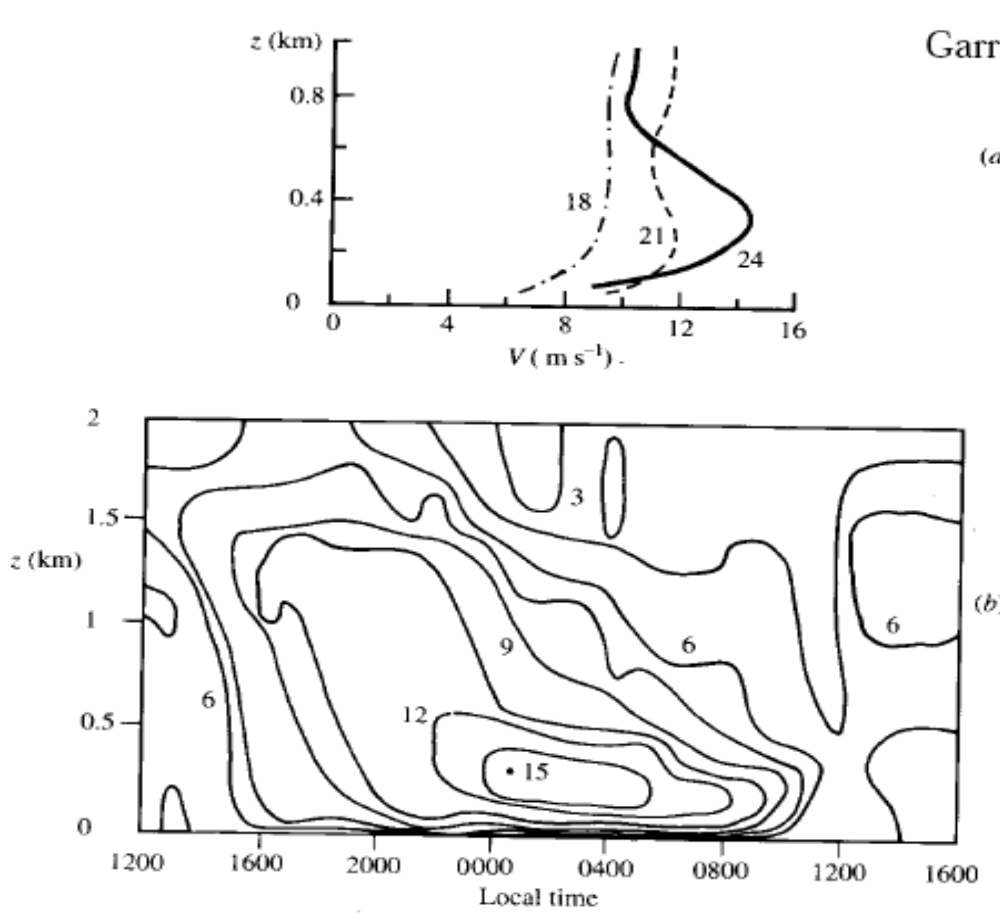

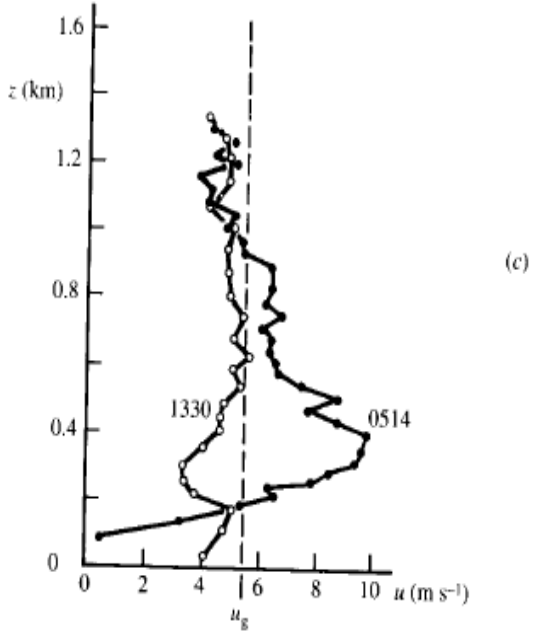

Fig. 6.18 Observations illustrating the formation of the nocturnal jet. (*a*) Wind-speed profiles on day 13 of WANGARA, local times indicated. (*b*) Height–time cross-section of wind speed (in $m\,s^{-1}$) on days 13/14 at WANGARA. Isopleths of wind speed are drawn at $1.5\,m\,s^{-1}$ intervals. (*c*) Profiles of the u-component of the wind velocity, with the x-axis along the geostrophic wind direction, for mid-afternoon (1330 UT, 6 August, 1974) and early morning (0514, 7 August, 1974) near Ascot, England. After Thorpe and Guymer (1977), *Quarterly Journal of the Royal Meteorological Society*.

Lecture13. The stable BL (Garratt 6.2)

The stable nocturnal BL (NBL) has proved one of the more difficult types of BL to understand and model. The boundary layer tends to be only 50-300 m deep. Turbulence tends to be intermittent and gravity-wave like motions are often intermingled with turbulence, especially in the upper part of the boundary layer. Radiative cooling in the air often has a comparable effect on the stratification to the turbulence itself, reaching 1 K hour^{-1} or more in the lowest 50-100 m (by comparison, a downward heat flux of H_0 = -10 W m^{-2} out of a NBL h = 100 m would cool it at a rate $dq/dt)_{turb}$ = $H_0/\rho c_p h$ = 10^{-4} K s^{-1} = 0.3 K hr^{-1}. Even the largest turbulent eddies do not span the entire BL so there is a tendency to layering of chemicals and aerosols within the BL, especially in the upper part of the BL where turbulence is weakest. Wind profiles are much less well-mixed at night than during the daytime convective BL.

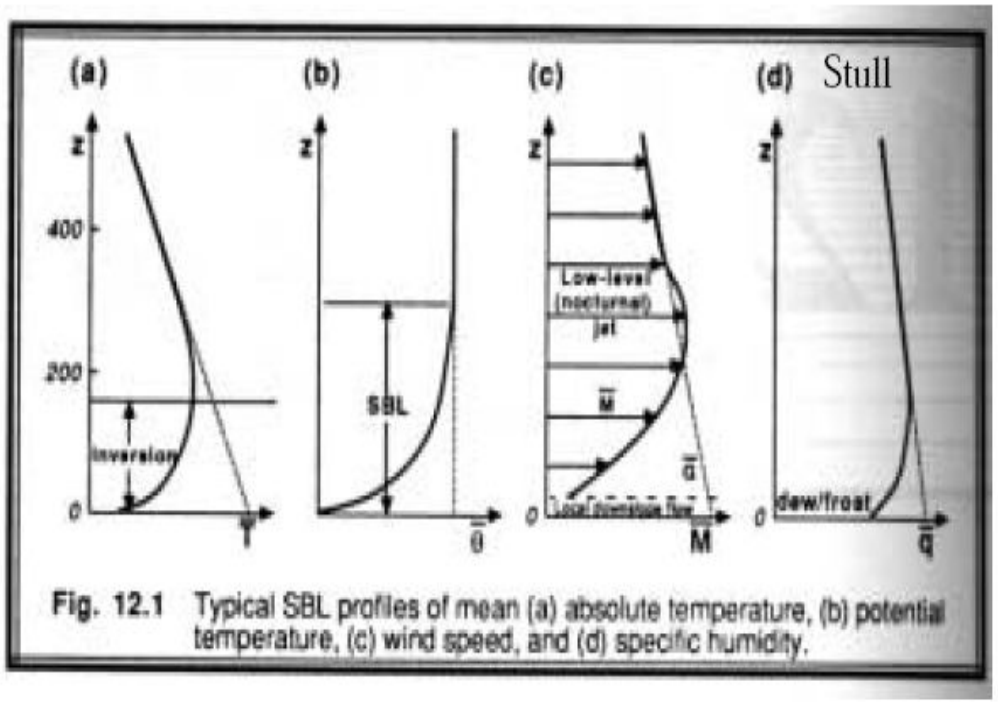

Fig. 12.1 Typical SBL profiles of mean (a) absolute temperature, (b) potential temperature, (c) wind speed, and (d) specific humidity.

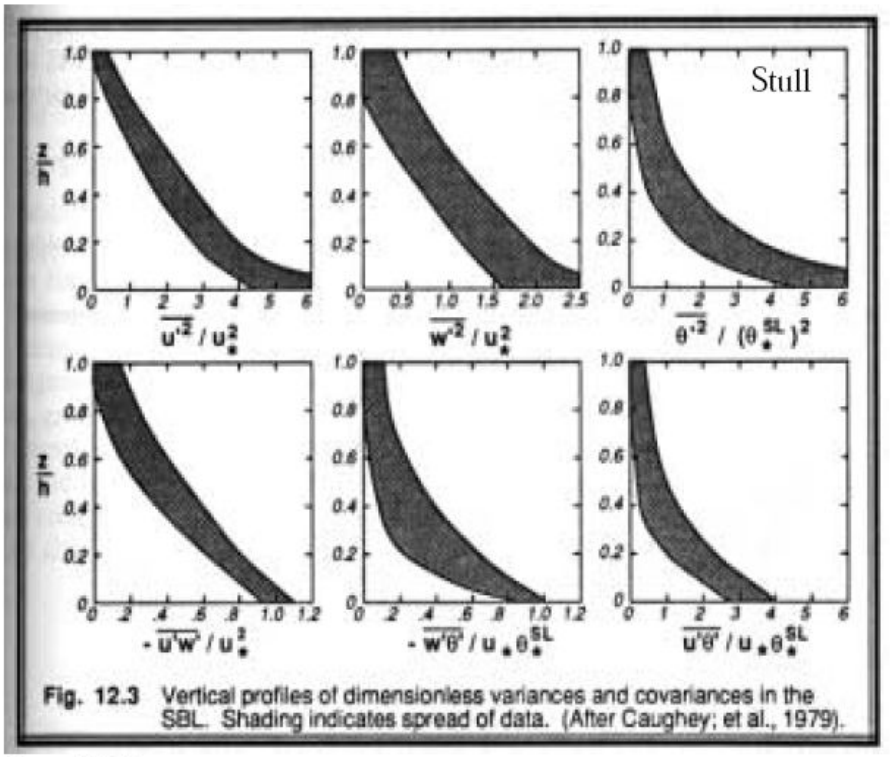

Fig. 12.3 Vertical profiles of dimensionless variances and covariances in the SBL. Shading indicates spread of data. (After Caughey; et al., 1979).

In an NBL, turbulence decreases sharply with height.

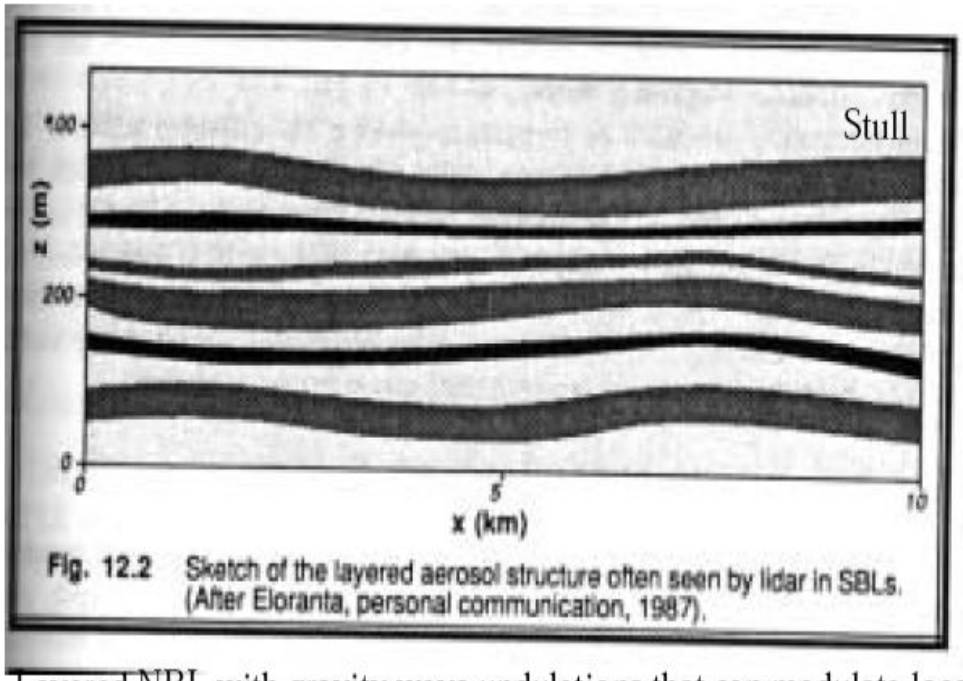

Fig. 12.2 Sketch of the layered aerosol structure often seen by lidar in SBLs. (After Eloranta, personal communication, 1987).

Layered NBL with gravity wave undulations that can modulate local shear, stratification, and hence turbulence.

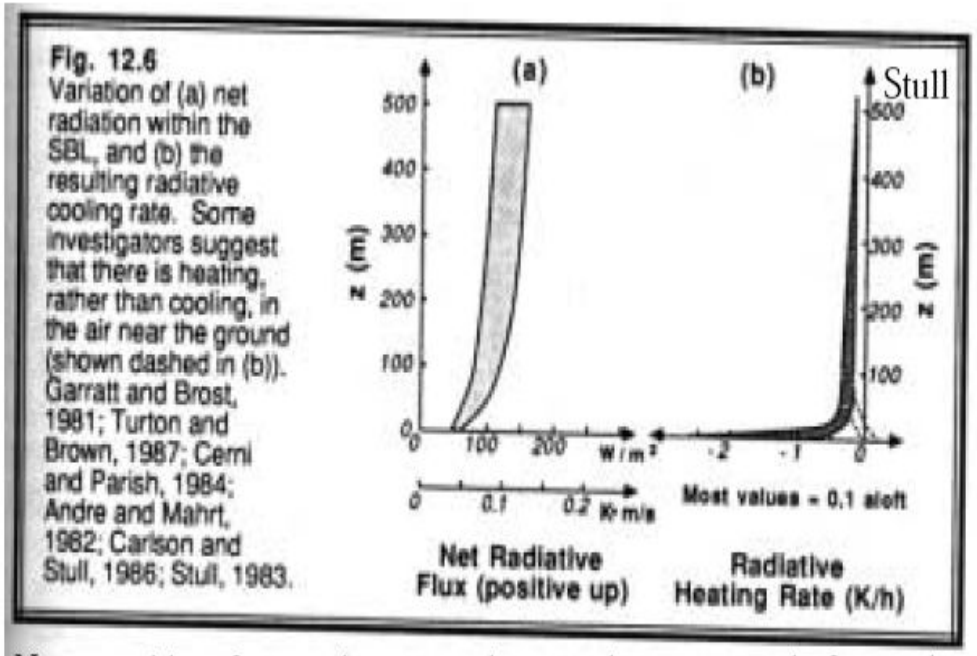

Near a cold surface, radiative cooling can be surprisingly fast and helps maintain a stable stratification.

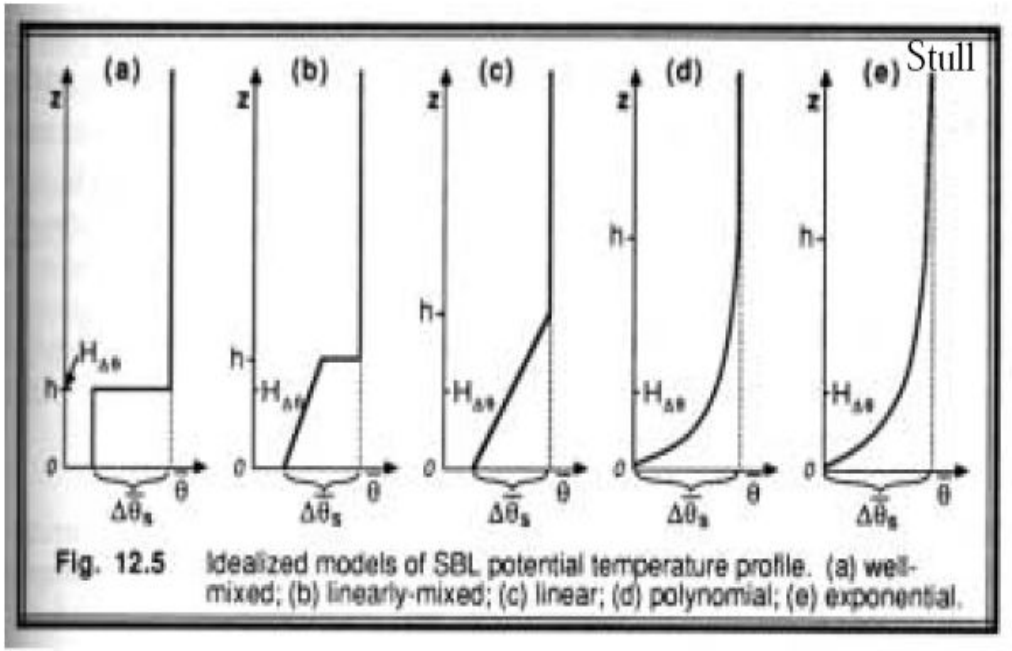

Fig. 12.5 Idealized models of SBL potential temperature profile. (a) well-mixed; (b) linearly-mixed; (c) linear; (d) polynomial; (e) exponential.

(b) typifies strong-wind NBL, (d) a weak-wind NBL under clear sky.

An idealized NBL model

One illuminating theoretical idealization is a NBL of constant depth driven by surface cooling only (Nieuwstadt 1984, *J. Atmos. Sci.*, **41**, 2202-2216). In practice, this is most realistic when winds are strong, producing sufficient turbulence to make substantial downward buoyancy fluxes that are much larger than the radiative flux divergence across the NBL (which is typically less than 10 W m^{-2}). We take the friction velocity u_*, the geostrophic wind U_g (taken to be in the $+x$ direction), and the Coriolis parameter f as given. (In a practical application we would likely know the surface roughness length z_0, not u_*, but we could use the solution below to relate these two parameters). We assume:

(i) The entire BL, extending up to a fixed but unknown height h, is cooling at the same rate, and maintains fixed vertical profiles of stratification and wind.

(ii) No turbulence at the top of the BL

(iii) Within the bulk of the BL (above the surface layer), the sink of TKE due to buoyancy fluxes is assumed to be a fixed fraction Rf ≈ 0.2 of the shear production of TKE. The remaining fraction (0.8) of the shear-produced TKE goes to turbulent dissipation, as transport is observed to be negligible. This is the same as saying that the flux Richardson number Rf = 0.2.

(iv) No radiative cooling within the BL

(v) The (unknown) Obuhkov length L is assumed much smaller than the boundary layer depth. Hence, the largest eddies have a depth which is order of L, since deeper eddies do not have enough TKE to overcome the stratification by the scaling arguments we made in discussing the z-less scaling at $z>>L$ when we discussed Monin-Obhukov theory.

(vi) The eddies act as an unknown, height-dependent eddy viscosity and diffusivity $K_m = K_h$ as suggested by Monin-Obuhkov theory. Hence the gradient Richardson number Ri = Rf, so is also 0.2 throughout the BL.

(vii) The BL is barotropic.

Scaling

Note that one could also use first-order closure on this problem instead of invoking assumptions (iii), (v) and (vi) about the eddies and their transports. This would give a largely similar answer as long as the lengthscale in the first-order closure was on the order of L through most of the boundary layer depth, and could also be used to relax the assumptions of steadiness, uniform cooling rate, no radiative cooling, and no thermal wind. However, the equations would not permit a closed-form solution which displays the parametric dependences clearly. We first scale the steady-state momentum equations, then use a clever approach to solve them.

Assumptions (i) and (ii) imply that if the (unknown) surface buoyancy flux is $B_0 < 0$, then

$$B(z) = \overline{w'b'} = B_0(1 - z/h) \tag{1}$$

The steady-state BL momentum equations are

$$-f(v - v_g) = -\partial/\partial z(\overline{u'w'}) \tag{2}$$

$$f(u - u_g) = -\partial/\partial z(\overline{v'w'}) \tag{3}$$

If {} indicates 'scale of', the above assumptions imply:

$$\{u'\} = \{v'\} = \{w'\} = u_*$$

$$\{K_m\} = \{\text{eddy velocity scale}\}\{\text{eddy lengthscale}\} = u_*L$$

If {} indicates 'scale of', the above assumptions imply:

$$\{u'\} = \{v'\} = \{w'\} = u_*$$

$$\{K_m\} = \{\text{eddy velocity scale}\}\{\text{eddy lengthscale}\} = u_* L$$

$$\Rightarrow \{\partial u/\partial z\} = \{\overline{u'w'}\}/\{K_m\} = u_*^2/u_* L = u_*/L \quad \text{(similarly for } v\text{)}$$

$$\{\partial/\partial z\} = h^{-1}$$

To apply this scaling to (2)-(3), we differentiate them with respect to z, noting that the geostrophic wind is constant with respect to height by assumption (vii):

$$-f\partial v/\partial z = -\partial^2/\partial z^2(\overline{u'w'}) \tag{4}$$

$$f\partial u/\partial z = -\partial^2/\partial z^2(\overline{v'w'}) \tag{5}$$

Scaling the two sides of (4), we find

$$\{f\partial v/\partial z\} = fu_*/L = \{\partial^2/\partial z^2(\overline{u'w'})\} = u_*^2/h^2.$$

The same scaling holds for (5). This implies a scaling for BL depth h:

$$h = \gamma_c(u_* L/f)^{1/2} \tag{6}$$

where γ_c is an as yet unknown proportionality constant.

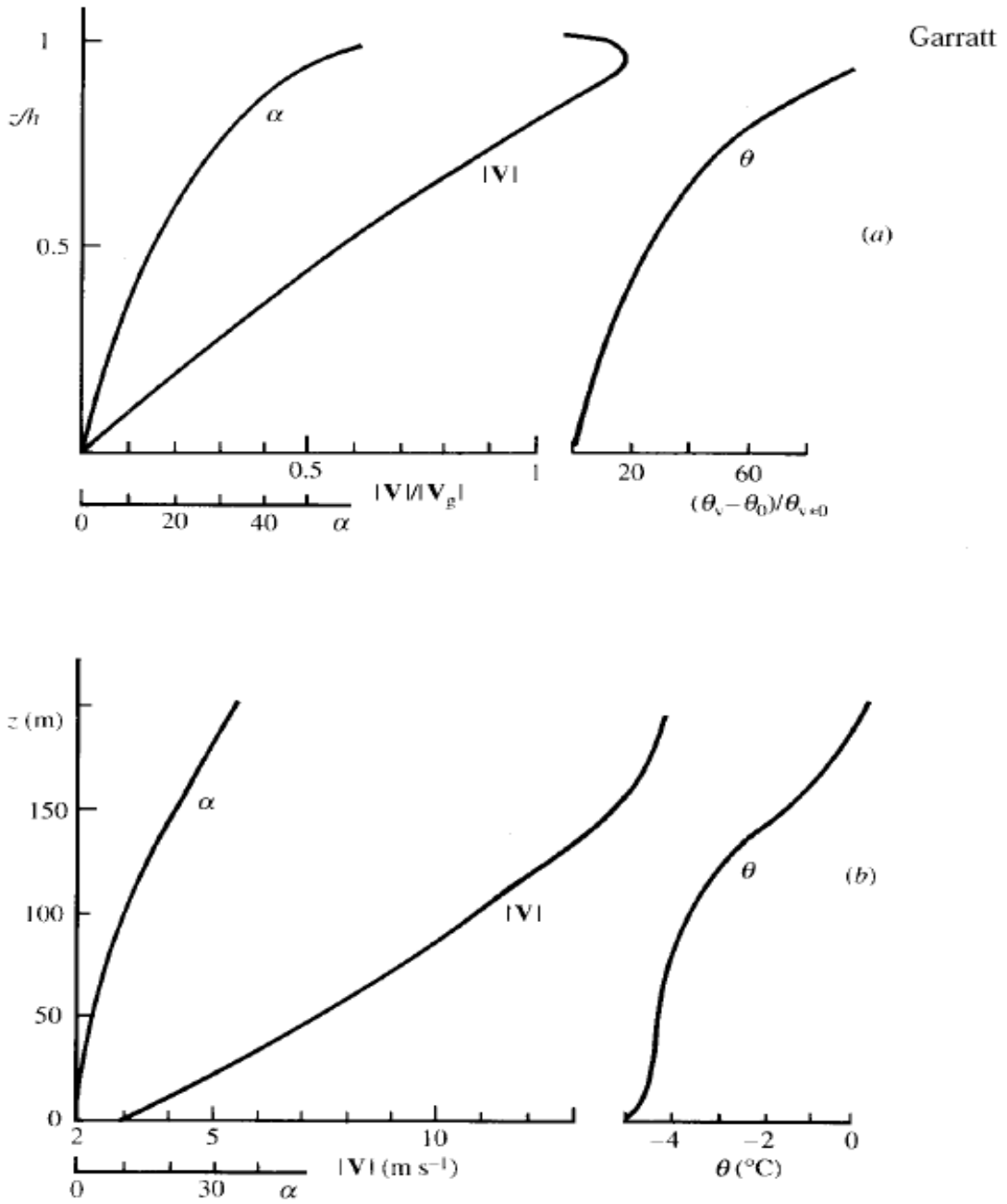

Fig. 6.15 (*a*) Predicted values of cross-isobar flow and normalized wind speed (Eq. 6.68) and of normalized temperature difference (Eq. 6.69) as functions of normalized height. (*b*) Observations from Cabaow of cross-isobar flow angle, wind speed and temperature as functions of height in the NBL. From Nieuwstadt (1985), by permission of the Oxford University Press.

Sloping terrain has a large influence on stable boundary layers. The cold dense air near the surface is now accelerated by the downslope component $b \sin \alpha$ of its buoyant acceleration (α is the slope angle and $b < 0$ is the buoyancy of air within the BL relative to above-BL air at the same height). Viewed in terrain-parallel coordinates, $b \sin \alpha$ is like an effective pressure gradient force, which is strongly height-dependent since b depends on z. In this sense, the slope acts similar to a thermal wind (which would also be associated with a height dependent PGF) . Slopes of as little as 2 in 1000 can have an impact on the BL scaling.

As the slope increases, or BL stability increases, the velocity profile is increasingly determined by drag created by turbulent mixing with air above rather than surface drag. As for the NBL, the BL is typically 10s to 100s of m thick. Over glaciers, katabatic winds often occur during the day as well as during the night, since the net radiation balance of a high-albedo surface is negative even during much of the day, and evaporative cooling due to surface snowmelt can also stabilize the air near the surface. On the coast of Antarctica, persistent katabatic flows down from the interior ice-caps can produce surface winds in excess of 50 m s^{-1}.

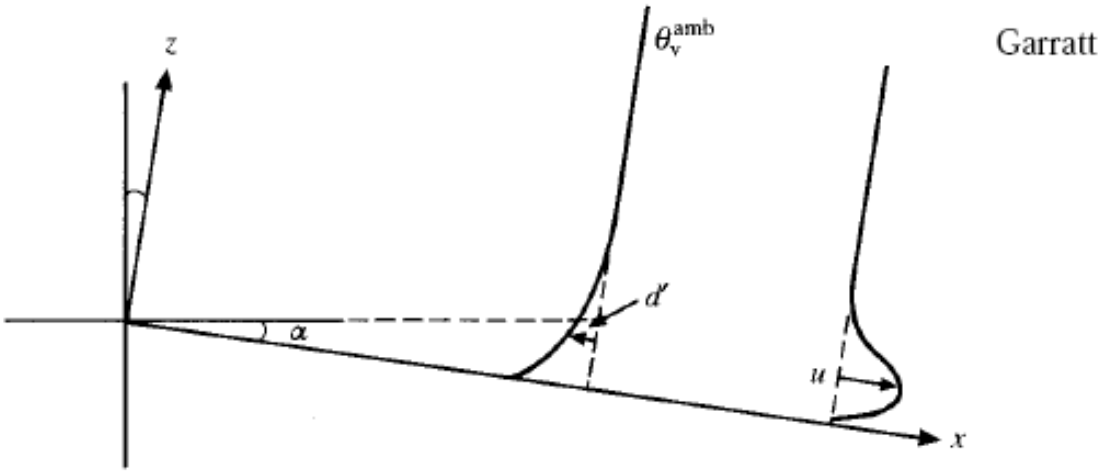

Fig. 6.22 Schematic representation of the downslope flow typical of night-time flow under light wind, clear sky conditions. Here, α is the slope angle and d' is the θ deficit of the flow relative to the ambient field.

Vortices in a stratified layer with horizontal shear

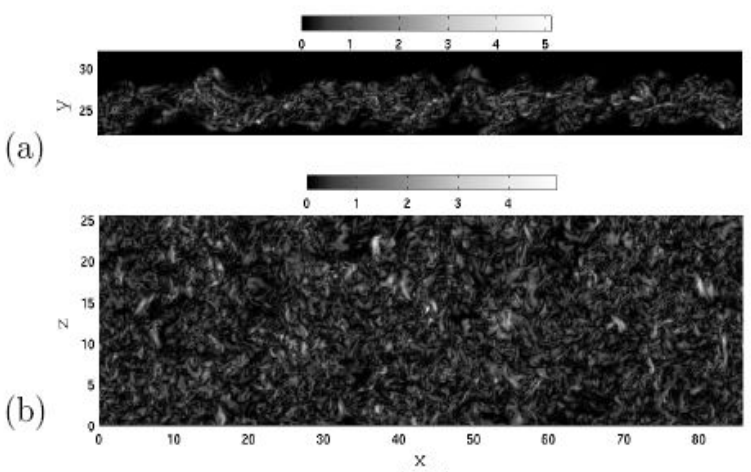

Figure 1: Vertical vorticity, $|\omega_z|$, in unstratified case. Part (a) is a horizontal cut at $z = 12.7$ and (b) is a vertical cut at $y = 25.7$, both taken from data at $t = 64.8$.

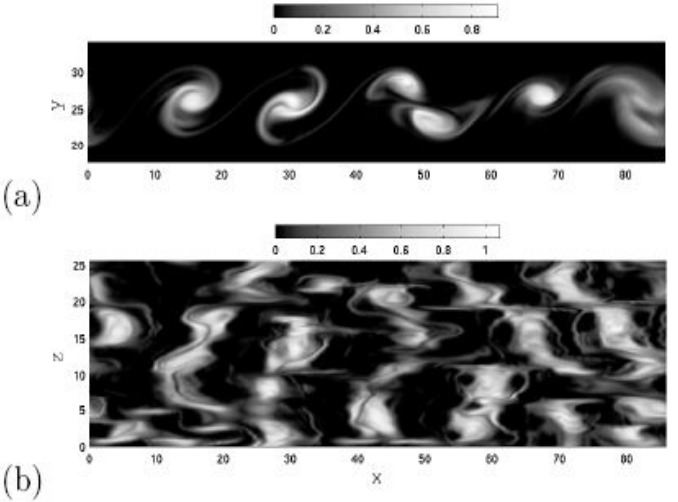

Figure 2: Vertical vorticity, $|\omega_z|$, in a case with large N. Part (a) and (b) are horizontal and vertical cuts, respectively, same locations as in Fig. 1. $t = 64.8$ and $Ri_b = 33$.

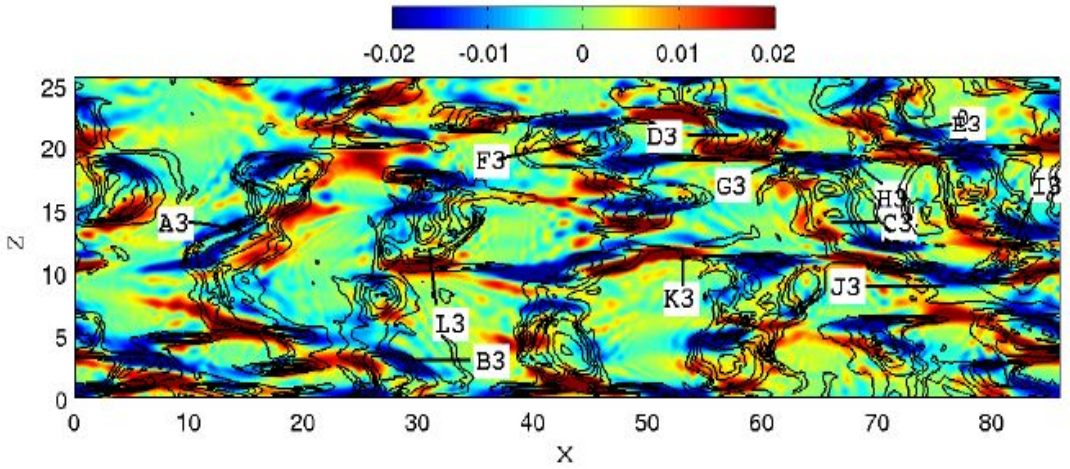

Figure 3: Density perturbation field (red denotes heavier and blue lighter fluid) for case A5 with ω_z contours overlapped, center y plane at a late time, $t = 79.8$, when $Ri_b = 45$.

GTP Workshop on
Coherent Structures in Atmosphere and Ocean
at NCAR, 11-14 July 2005, Boulder, CO, USA

Turbulence in Strongly-Stratified Fluids

Jim Riley,[1] Steve de Bruyn Kops,[2] and Kraig Winters[3]
[1] *University of Washington, Seattle, Washington, 98195, USA*
[2] *University of Massachusetts, Amherst, Massachusetts, 01003, USA*
[3] *Scripps Institution of Oceanography, La Jolla, California, 92093, USA*

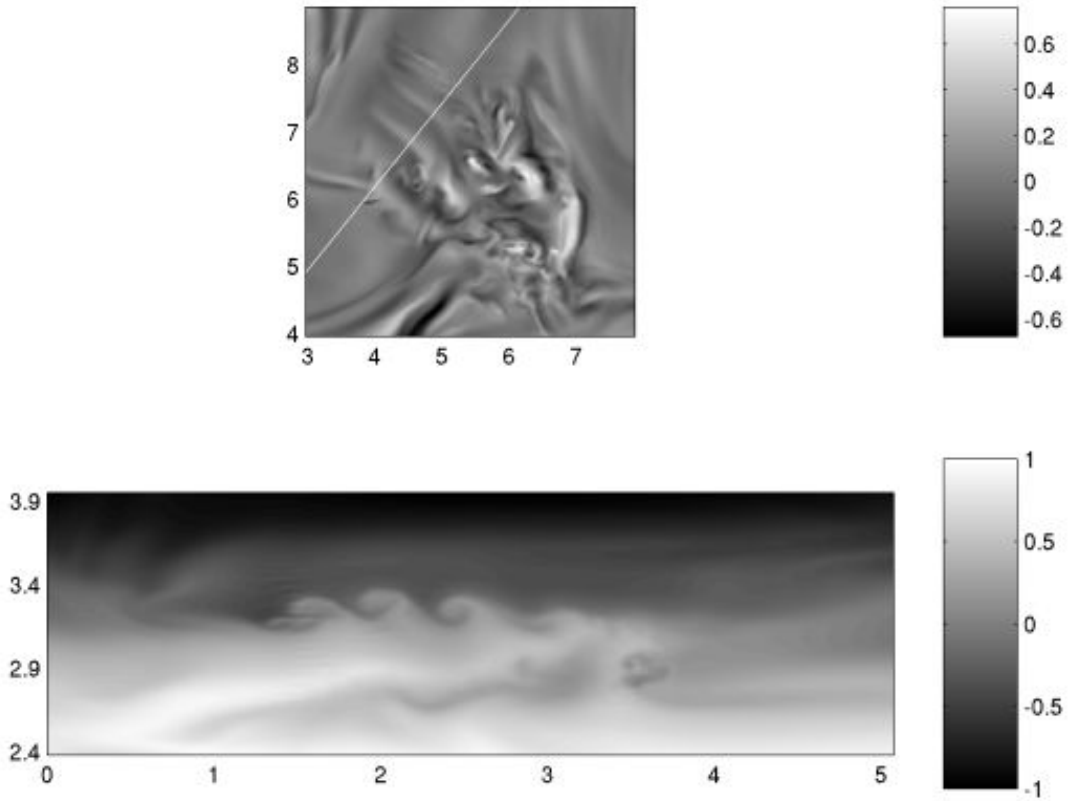

Figure 1: *The top panel shows part of a horizontal slice through the w field. the white dashed line gives the orientation of a vertical slice through the horizontal plane. The bottom panel shows the density field on that vertical slice.*

COHERENT STRUCTURES IN THE ATMOSPHERIC SURFACE LAYER UNDER STABLE AND UNSTABLE CONDITIONS

B. M. KOPROV, V. M. KOPROV, T. I. MAKAROVA and G. S. GOLITSYN
A. M. Obukhov Institute of Atmospheric Physics, Russian Academy of Sciences, Pyzhevsky per. 3, Moscow 119017, Russia

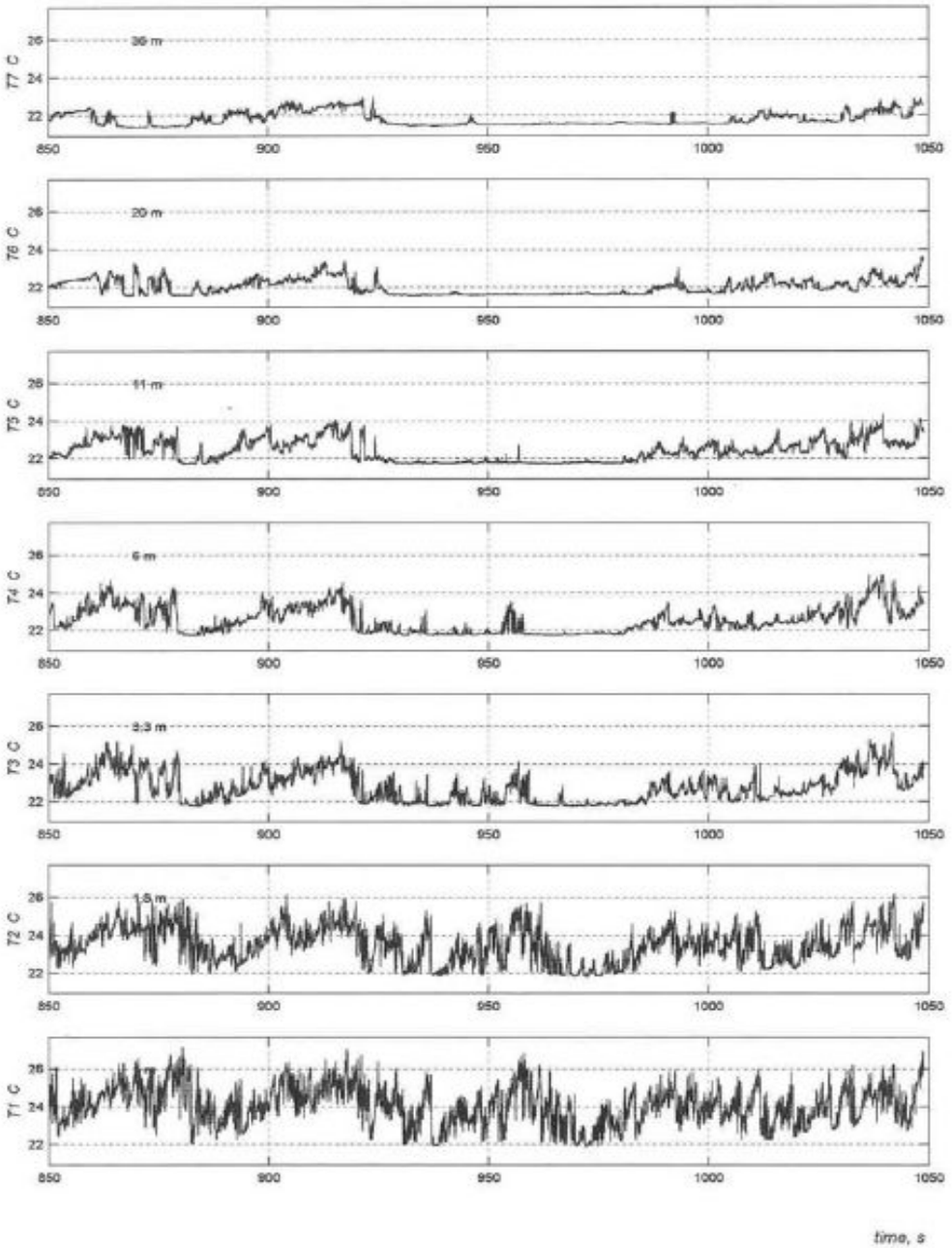

Figure 1. A fragment of synchronous traces of temperature at seven levels 1, 1.8, 3.3, 6, 11, 20 and 36 m under unstable conditions. $U = 6.3$ m s^{-1}, $|L| = 32$ m, 1448 local time.

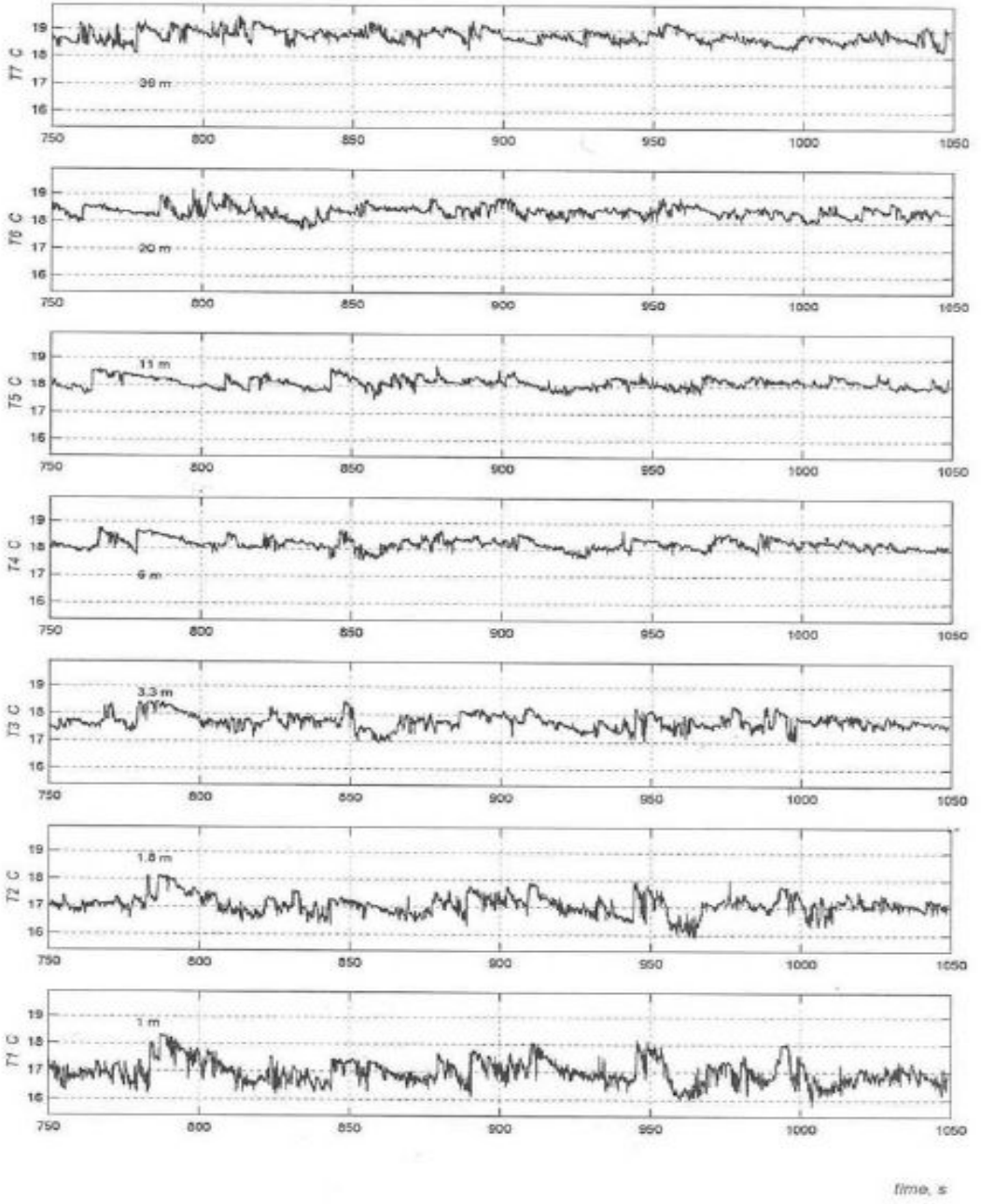

Figure 4. A fragment of synchronous traces of absolute temperatures in nighttime under inversion conditions.

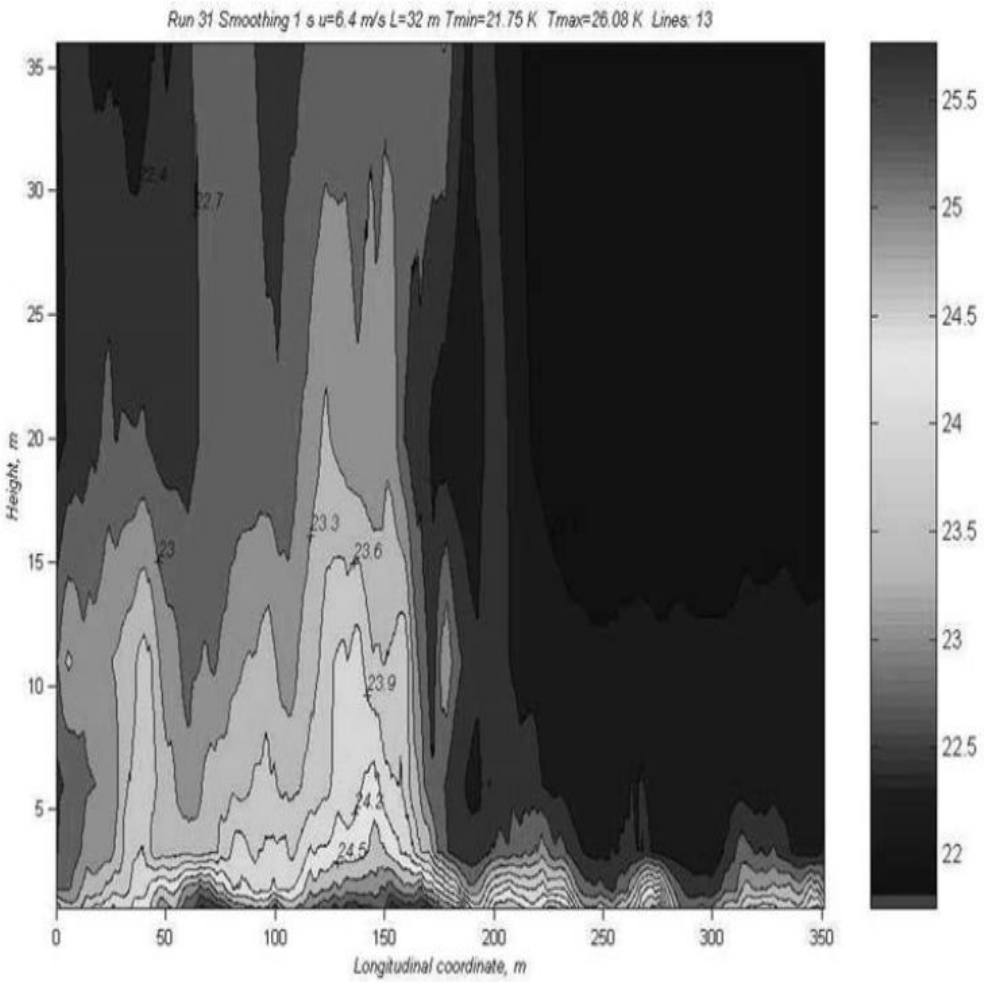

Figure 3. The temperature field within the time interval including the back side of the structure (near $t = 918$ s in the Figure 1) and a quiet interval. Numbers are the temperatures at corresponding surfaces.

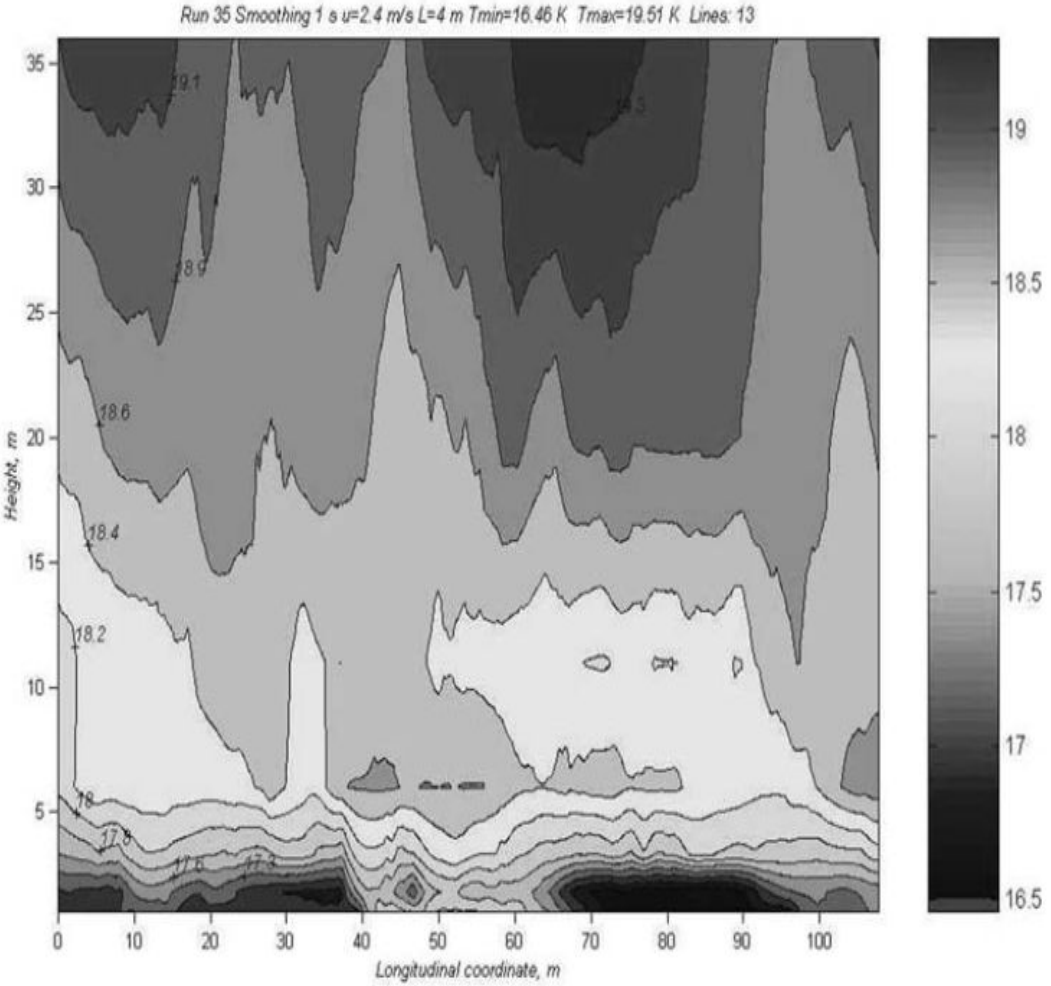

Figure 5. The temperature field in inversion conditions. $u = 2.4$ m s^{-1}, $|L| = 4$ m, time 2200. The isotherms are drawn with the interval of 0.2 K.